Appendix A
Calculation of the Circulation Time

The two-dimensional simplification of Eq. (5.4.1) into Eq. (5.4.2) is valid for a plane (xy). Since the PIV measurements were also obtained on a plane, Eq. (5.4.2) gives the circulation times on this plane. If 2D data were used in Eq. (5.4.1), this would assume a certain velocity profile along the channel depth (axisymmetric flow). This may not be wrong but it does involve an assumption, as 3D experimental data were not obtained. The use of Eq. (5.4.1) will only lead to higher values of the circulation time compared to Eq. (5.4.2), i.e. $\tau_{3\text{-}D} = 1.6\tau$, without changing any trends or their significance. This is because Eq. (5.4.1) represents an average along the z direction; while Eq. (5.4.2) represents the mid-plane only where velocities are expected to be higher (i.e. circulation time is expected to be lower). This slight difference can be seen in Fig. A.1 below where the non-dimensional circulation times found from both equations are compared.

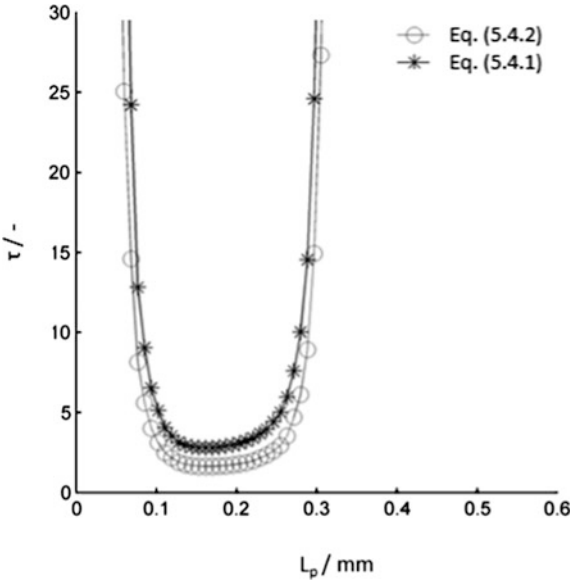

Fig. A.1 Comparison between non dimensional circulation time profiles found using Eqs. (5.4.1) and (5.4.2) for the same experimental conditions

D.A. Tsaoulidis, *Studies of Intensified Small-scale Processes for Liquid–Liquid Separations in Spent Nuclear Fuel Reprocessing*, Springer Theses, DOI 10.1007/978-3-319-22587-6

Appendix B
Circulation Patterns at the Bend of the Channel

Circulation patterns were also obtained at the bend of the channel for different orientations of the plug centre, using both liquids (i.e. ionic liquid and water) as carrier fluid. It was found that the vortex internal symmetry is broken at the channel bend regardless which liquid is the carrier fluid, as shown in Fig. B.1, where the stretching and the folding of the fluid are clearly observable and a single main vortex is revealed toward the inner meander of the channel. This effect, combined with the reorientation of the fluid given by a sequence of bends, triggers a more effective mixing across the transversal direction (y).

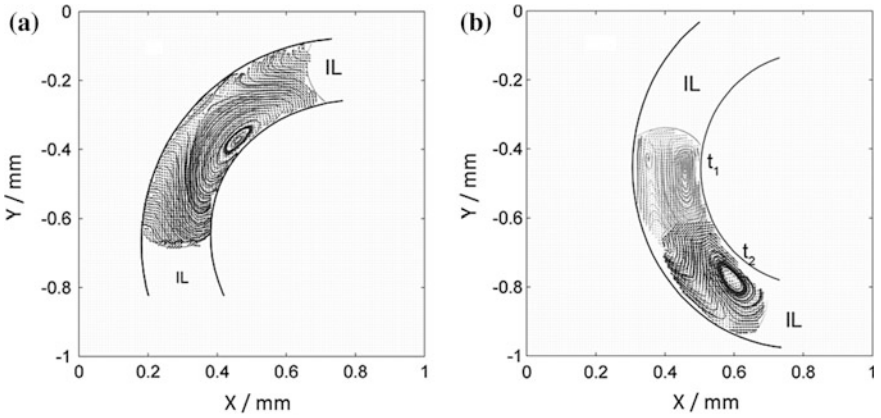

Fig. B.1 Ensemble averaged circulation pattern within a single water plug at a bend for different orientations of the plug centre (i.e. 0, t_1, and 45 degree, t_2), when water (**a**) and ionic liquid (**b**) was the carrier. Sixty instantaneous fields were averaged

D.A. Tsaoulidis, *Studies of Intensified Small-scale Processes for Liquid–Liquid Separations in Spent Nuclear Fuel Reprocessing*, Springer Theses, DOI 10.1007/978-3-319-22587-6

Appendix C
MATLAB Code for Image Processing

The high resolution images acquired with the high speed camera were used for the measurements of the hydrodynamics and mixing characteristics as discussed in Sect. 3.5.1.2. A script that allocates the plugs in an initial position and renames the files so they can be used in Insight 4G is presented.

```
%%%Move plug to initial position
clear all
close all
clc

%path of data file
path='E:\hydrop\2mm\ratio1\0.01m_s\pl\New folder (2)\';
mkdir(path,'newimage2')
path2=strcat(path,'newimage2\');

imgs=dir(strcat(path,'*.tif')); % Change to jpg when the format is
different

%initialization/allocation
if(mod(length(imgs),2)~=0),
    error('not enough number of pics to put them in pairs!');
end
col=length(imgs)/2;
imgLA=cell(1,col);
imgLB=cell(1,col);
i=0;  %counter
j=0;

for k=1:numel(imgs)

    if(mod(k, 2) == 1),
        i=i+1;
        imgLA{i} = imread(strcat(path,imgs(k).name));
        if(k==1),
            [a, b]=size(imgLA{k});  %check the size of the image for
allocation , assume each image is the same size!
        end
    else
        j=j+1;
        imgLB{j} = imread(strcat(path,imgs(k).name));
    end

end

n=input('give the pixels shift: \n');
```


D.A. Tsaoulidis, *Studies of Intensified Small-scale Processes for Liquid–Liquid Separations in Spent Nuclear Fuel Reprocessing*, Springer Theses, DOI 10.1007/978-3-319-22587-6

```
imgLA_new=cell(1,col);
imgLA_new(:) = {zeros(a, b)};
%imgLA_new=uint8(imgLA_new);
imgLB_new=cell(1,col);
imgLB_new(:) = {zeros(a, b)};
%imgLB_new=uint8(imgLB_new);

for l=1:col,

    for m=1:b-((col-1)*2*n),
       imgLA_new{l}(:,m)=imgLA{l}(:,m+(l-1)*2*n);
       imgLB_new{l}(:,m)=imgLB{l}(:,m+(l-1)*2*n);
    end
end

for h=1:col,

    imgLA_new{h}=uint8(imgLA_new{h});
    imgLB_new{h}=uint8(imgLB_new{h});

end

%%save
new_name={imgs(1).name(1:end-7)}; %cut last 5 or 7

for h=1:col,

imwrite(imgLA_new{h},strcat(path2,new_name,sprintf('%03d',h),'.LA.tif'),'ti
f');

imwrite(imgLB_new{h},strcat(path2,new_name,sprintf('%03d',h),'.LB.tif'),'ti
f');

end
```

Appendix D
Sensitivity Analysis of Diffusion Coefficient

The diffusion coefficients of dioxouranium(VI) ions in the ionic liquid phase was obtained based on literature correlations, since no exact information exists. Diffusion coefficients of dioxouranium in ionic liquids in literature (Giridhar et al. 2007; Liu et al. 2011) varied from 10^{-12} to 10^{-10} m^2 s^{-1}. However, it can be seen that the diffusion coefficient has negligible effect on the mass transfer within that range (Fig. D.1).

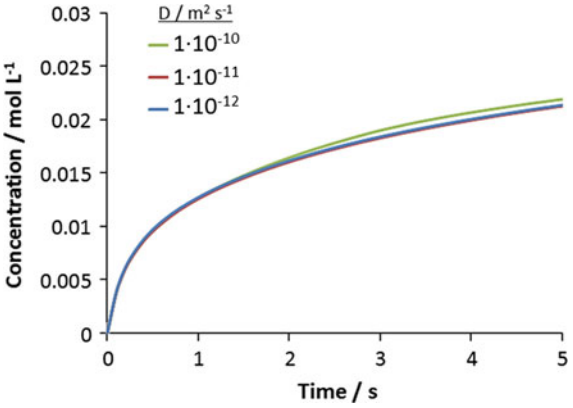

Fig. D.1 Concentration of dioxouranium(VI) in the ionic liquid phase as a function of time for different diffusion coefficients

D.A. Tsaoulidis, *Studies of Intensified Small-scale Processes for Liquid–Liquid Separations in Spent Nuclear Fuel Reprocessing*, Springer Theses, DOI 10.1007/978-3-319-22587-6

Appendix E
Numerical Model Report

A short report for the numerical model developed in Chap. 7 is provided. The simulation environment is Comsol Multiphysics 4.4.

E.1. Global Definitions

E.1.1. Parameters

Name	Expression	Description
K	3.16	Partition coefficient
M	10e1[m/s]	Stiff-spring velocity
u_TP	0.036–0.039[m/s]	Experimental plug velocity
c0	0.05[mol/L]	Initial concentration in the droplet
t_step	5[ms]	Step time

E.2. Model

E.2.1. Definitions

Name	Expression	Description
c_all	c1	Concentration in droplet
c_all	c2	Concentration in IL phase
N_partition	M*(c2—K*c1)*step1(t/t_step)	Flux across boundary
n_droplet	int_droplet(c1)	Moles of solute (droplet)
n_flow	int_flow(c2)	Moles of solute (flow)
n_tot	n_droplet + n_flow	Moles of solute (total)

D.A. Tsaoulidis, *Studies of Intensified Small-scale Processes for Liquid–Liquid Separations in Spent Nuclear Fuel Reprocessing*, Springer Theses, DOI 10.1007/978-3-319-22587-6

Integration

Coupling type	Integration
Operator name	int_flow

Source selection

Geometric entity level	Domain
Selection	Domain 1

Boundary System 1

Coordinate system type	Boundary system
Identifier	sys1

Settings

Name	Value
Coordinate names	{t1, to, n}
Create first tangent direction from	Global Cartesian

E.2.2. Geometry

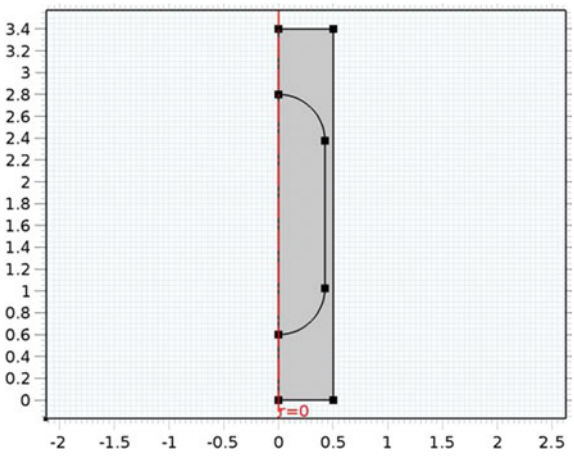

Units

Length unit	mm
Angular unit	deg

Geometry statistics

Property	Value
Space dimension	2
Number of domains	2
Number of boundaries	9
Number of vertices	8

E.2.3. Laminar Flow

Selection

Geometric entity level	Domain
Selection	Domains 1–2

Equations

$$\rho(\mathbf{u}\cdot\nabla)\mathbf{u} =$$
$$\nabla\cdot\left[-p\mathrm{I} + \mu\left(\nabla\mathbf{u} + (\nabla\mathbf{u})^T\right)\right] + \mathbf{F}$$
$$\rho\nabla\cdot\mathbf{u} = 0$$

Settings

Description	Value
Discretization of fluids	P1 + P1
Value type when using splitting of complex variables	{Real, Real, Real, Real, Real, Real, Real, Real, Real}
Neglect inertial term (Stokes flow)	Off
Swirl flow	Off

Variables

Name	Expression	Unit	Description	Selection
spf.rho	model.input.rho	kg/m^3	Density	Domain 1
spf.mu	model.input.mu	Pa*s	Dynamic viscosity	Domain 1
spf.divu	ur + if(abs (r) < 0.0010*h,ur, u/r) + wz	1/s	Divergence of velocity field	Domain 1
spf.sr	sqrt(0.5*(4*ur^2 + 2* (uz + wr)^2 + 4*if(abs (r) < 0.0010*h,ur,u/r) ^2 + 4*wz^2) + eps)	1/s	Shear rate	Domain 1
spf.Fr	0	N/m^3	Volume force, r component	Domain 1
spf.Fphi	0	N/m^3	Volume force, phi component	Domain 1
spf.Fz	0	N/m^3	Volume force, z component	Domain 1
spf.U	sqrt(u^2 + w^2)	m/s	Velocity magnitude	Domain 1
spf.vorticityr	0	1/s	Vorticity field, r component	Domain 1
spf.vorticityphi	−wr + uz	1/s	Vorticity field, phi component	Domain 1
spf.vorticityz	0	1/s	Vorticity field, z component	Domain 1
spf.vort_magn	sqrt(spf. vorticityr^2 + spf. vorticityphi^2 + spf. vorticityz^2)	1/s	Vorticity magnitude	Domain 1
spf.cellRe	0.25*spf.rho*sqrt (emetric(u,w)/emetric2)/ spf.mu	1	Cell Reynolds number	Domain 1
spf.nu	spf.mu/spf.rho	m^2/s	Kinematic viscosity	Domain 1
spf.betaT	0	1/Pa	Isothermal compressibility coefficient	Domain 1
spf.T_stressr	2*spf.mu*ur*spf. nrmesh + spf.mu* (uz + wr)*spf. nzmesh − p*spf.nrmesh	N/m^2	Total stress, r component	Boundaries 2, 5–9
spf.T_stressphi	spf.nphimesh*(2*spf. mu*if(abs (r) < 0.0010*h,ur, u/r) − p)	N/m^2	Total stress, phi component	Boundaries 2, 5–9

(continued)

(continued)

spf.T_stressz	spf.mu*(wr + uz)*spf.nrmesh + 2*spf.mu*wz*spf.nzmesh − p*spf.nzmesh	N/m^2	Total stress, z component	Boundaries 2, 5–9
spf.K_stressr	spf.mu*(2*ur*spf.nrmesh + (uz + wr)*spf.nzmesh)	N/m^2	Viscous stress, r component	Boundaries 2, 5–9
spf.K_stressphi	2*spf.mu*if(abs(r) < 0.0010*h,ur,u/r)*spf.nphimesh	N/m^2	Viscous stress, phi component	Boundaries 2, 5–9
spf.K_stressz	spf.mu*((wr + uz)*spf.nrmesh + 2*wz*spf.nzmesh)	N/m^2	Viscous stress, z component	Boundaries 2, 5–9
spf.upwind_helpr	u	m/s		Domain 1
spf.upwind_helpphi	0	m/s		Domain 1
spf.upwind_helpz	w	m/s		Domain 1
spf.K_stress_tensorrr	2*spf.mu*ur	N/m^2	Viscous stress tensor, rr component	Domain 1
spf.K_stress_tensorphir	0	N/m^2	Viscous stress tensor, phir component	Domain 1
spf.K_stress_tensorzr	spf.mu*(wr + uz)	N/m^2	Viscous stress tensor, zr component	Domain 1
spf.K_stress_tensorrphi	0	N/m^2	Viscous stress tensor, rphi component	Domain 1
spf.K_stress_tensorphiphi	2*spf.mu*if(abs(r) < 0.0010*h,ur,u/r)	N/m^2	Viscous stress tensor, phiphi component	Domain 1
spf.K_stress_tensorzphi	0	N/m^2	Viscous stress tensor, zphi component	Domain 1
spf.K_stress_tensorrz	spf.mu*(uz + wr)	N/m^2	Viscous stress tensor, rz component	Domain 1
spf.K_stress_tensorphiz	0	N/m^2	Viscous stress tensor, phiz component	Domain 1
spf.K_stress_tensorzz	2*spf.mu*wz	N/m^2	Viscous stress tensor, zz component	Domain 1
spf.K_stress_tensor_testrr	2*spf.mu*test(ur)	N/m^2	Viscous stress tensor test, rr component	Domain 1

(continued)

(continued)

spf.K_stress_tensor_testphir	0	N/m^2	Viscous stress tensor test, phir component	Domain 1
spf.K_stress_tensor_testzr	spf.mu*(test(wr) + test(uz))	N/m^2	Viscous stress tensor test, zr component	Domain 1
spf.K_stress_tensor_testrphi	0	N/m^2	Viscous stress tensor test, rphi component	Domain 1
spf.K_stress_tensor_testphiphi	2*spf.mu*if(abs(r) < 0.0010*h,test(ur),test(u)/r)	N/m^2	Viscous stress tensor test, phiphi component	Domain 1
spf.K_stress_tensor_testzphi	0	N/m^2	Viscous stress tensor test, zphi component	Domain 1
spf.K_stress_tensor_testrz	spf.mu*(test(uz) + test(wr))	N/m^2	Viscous stress tensor test, rz component	Domain 1
spf.K_stress_tensor_testphiz	0	N/m^2	Viscous stress tensor test, phiz component	Domain 1
spf.K_stress_tensor_testzz	2*spf.mu*test(wz)	N/m^2	Viscous stress tensor test, zz component	Domain 1
spf.res_u	pr + spf.rho*u*ur + spf.rho*w*uz − (d(2*ur,r) + if(abs(r) < 0.0010*h,d(2*ur,r),2*ur/r) + d(uz + wr,z) − 2*if(abs(r) < 0.0010*h,ur,u/r)/r)*spf.mu − spf.Fr	N/m^3	Equation residual	Domain 1
spf.res_v	−spf.Fphi	N/m^3	Equation residual	Domain 1
spf.res_w	spf.rho*u*wr + pz + spf.rho*w*wz − (d(wr + uz,r) + if(abs(r) < 0.0010*h,d(wr + uz,r),(wr + uz)/r) + d(2*wz,z))*spf.mu − spf.Fz	N/m^3	Equation residual	Domain 1
spf.res_p	spf.rho*spf.divu	$kg/m^3 * s$	Pressure equation residual	Domain 1

Shape functions

Name	Shape function	Unit	Description	Shape frame	Selection
u	Lagrange (Linear)	m/s	Velocity field, r component	Material	Domain 1
w	Lagrange (Linear)	m/s	Velocity field, z component	Material	Domain 1
p	Lagrange (Linear)	Pa	Pressure	Material	Domain 1

Weak expressions

Weak expression			Integration frame	Selection
2*((p − spf.K_stress_tensorrr)*test(ur) − spf.K_stress_tensorrz*test(uz) + (p − spf.K_stress_tensorphiphi)*if(abs(r) < 0.0010*h,test(ur),test(u)/r) − spf.K_stress_tensorzr*test(wr) + (p − spf.K_stress_tensorzz)*test(wz))*pi*r			Material	Domain 1
2*(spf.Fr*test(u) + spf.Fz*test(w) − spf.rho*(ur*u + uz*w)*test(u) − spf.rho*(wr*u + wz*w)*test(w))*pi*r			Material	Domain 1
−2*spf.rho*spf.divu*test(p)*pi*r			Material	Domain 1
2*spf.crosswindns*pi*r			Material	Domain 1
2*spf.streamlinens*pi*r			Material	Domain 1
spf.uwallz	−u_TP	m/s	Velocity of moving wall, z component	Boundary 7

Periodic Flow Condition 1

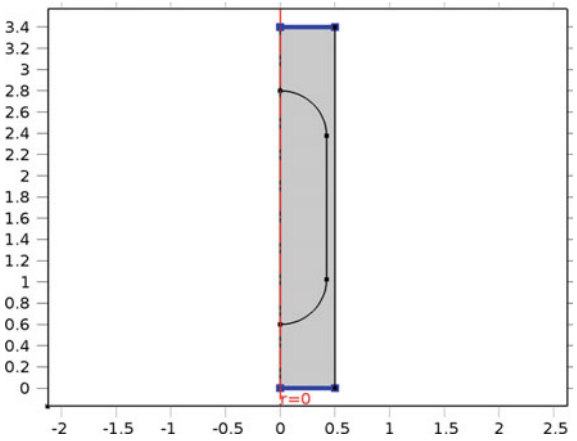

Selection

Geometric entity level	Boundary
Selection	Boundaries 2, 5

Equations

$$\mathbf{u}_{\text{source}} = \mathbf{u}_{\text{dest}}, \quad p_{\text{source}} = p_{\text{dest}}$$

Settings

Description	Value
Pressure difference	0
Apply reaction terms on	All physics (symmetric)
Use weak constraints	Off

Destination Selection 1

Geometric entity level	Boundary
Selection	Boundary 2

Pressure Point Constraint 1

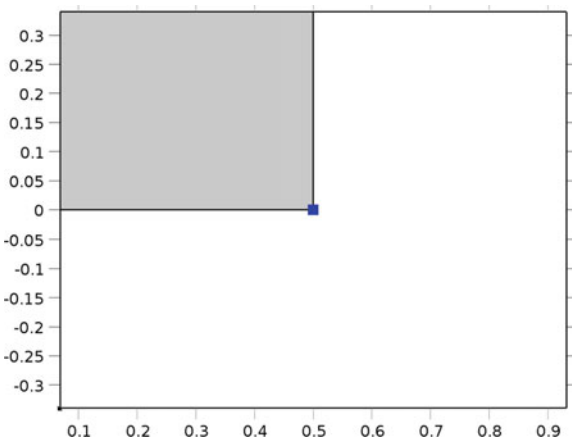

Selection

Geometric entity level	Point
Selection	Point 7

Settings

Description	Value
Pressure	1
Apply reaction terms on	All physics (symmetric)
Use weak constraints	Off

Variables

Name	Expression	Unit	Description	Selection
spf.p0	1	Pa	Pressure	Point 7

Shape functions

Constraint	Constraint force	Shape function	Selection
−p + spf.p0	test(−p + spf.p0)	Lagrange (Linear)	Point 7

E.2.4. Transport of Diluted Species

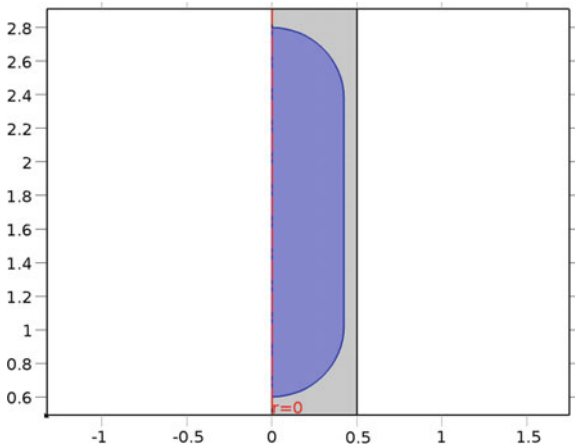

Selection

Geometric entity level	Domain
Selection	Domain 2

Equations

$$\frac{\partial c_i}{\partial t} + \nabla \cdot (-D_i \nabla c_i + \mathbf{u} c_i) = R_i$$
$$\mathbf{N}_i = -D_i \nabla c_i + \mathbf{u} c_i$$

Settings

Description	Value
Concentration	Linear
Compute boundary fluxes	On
Apply smoothing to boundary fluxes	On
Value type when using splitting of complex variables	Real
Migration in electric field	0
Convection	1
Convective term	Conservative form
Equation residual	Approximate residual
Enable space-dependent physics interfaces	0
Synchronize with COMSOL Multiphysics	

Convection-diffusion

Selection

Geometric entity level	Domain
Selection	Domain 2

Equations

$$\nabla \cdot (-D_i \nabla c_i + \mathbf{u} c_i) = R_i$$
$$\mathbf{N}_i = -D_i \nabla c_i + \mathbf{u} c_i$$

Settings

Description	Value
Velocity field	Velocity field (spf)
Electric potential	User defined
Electric potential	0
Diffusion coefficient	User defined
Diffusion coefficient	{{7e − 10[m^2/s], 0, 0}, {0, 7e − 10[m^2/s], 0}, {0, 0, 7e − 10[m^2/s]}}
Bulk material	None

Shape functions

Name	Shape function	Unit	Description	Shape frame	Selection
c1	Lagrange (Linear)	mol/*hboxm*^{3}	Concentration	Material	Domain 2

Weak expressions

Weak expression	Integration frame	Selection
2*(−d(c1,t)*test(c1) − (chds.Drr_c1*c1r + chds.Drz_c1*c1z)*test(c1r) − (chds.Dzr_c1*c1r + chds.Dzz_c1*c1z)*test(c1z))*pi*r	Material	Domain 2
2*c1*(chds.u*test(c1r) + chds.w*test(c1z))*pi*r	Material	Domain 2
2*chds.cbf_c1*test(c1)*pi*r	Material	Boundaries 3, 6, 8–9
2*chds.streamline*pi*r	Material	Domain 2
2*chds.crosswind*pi*r	Material	Domain 2

Periodic Condition

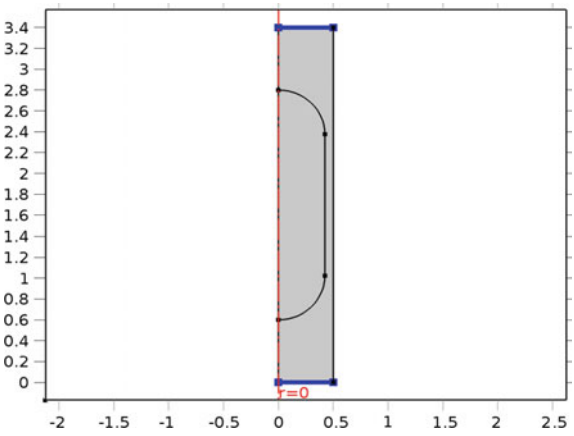

Equations

$$C_{i,\mathrm{src}} = C_{i,\mathrm{dst}}$$
$$-\mathbf{n}_{\mathrm{src}} \cdot \mathbf{N}_{i,\mathrm{src}} = \mathbf{n}_{\mathrm{dst}} \cdot \mathbf{N}_{i,\mathrm{dst}}$$

E.2.5. Meshes

Mesh statistics

Property	Value
Minimum element quality	0.3305
Average element quality	0.9577
Triangular elements	48900
Quadrilateral elements	702
Edge elements	1418
Vertex elements	8

Free Triangular (settings)

Name	Value
Maximum element size (μm)	1.6–3
Minimum element size (μm)	0.1–0.4
Curvature factor	0.25
Curvature factor	Off
Resolution of narrow regions	Off
Maximum element growth rate	1.25
Maximum element growth rate	Off
Predefined size	Finer
Custom element size	Custom

References

Liu, C., Shang, J. & Zachara, J. M. (2011). Multispecies diffusion models: A study of uranyl species diffusion. *Water Resources Research,* 47.

Giridhar, P., Venkatesan, K., Srinivasan, T., & Rao, P. (2007). Electrochemical behavior of uranium (VI) in 1-butyl-3-methylimidazolium chloride and thermal characterization of uranium oxide deposit. *Electrochimica Acta, 52*, 3006–3012.

Conferences

Tsaoulidis D., Dore V., Plechkova N., Seddon K.R., Angeli P., 2011. Liquid-liquid flows in Microchannels. In proceedings of the 3rd Micro and Nano Flows Conference, 22–24 August, Thessaloniki, Greece

Tsaoulidis D., Dore V., Angeli, P., 2012. Microchannel extractions using ionic liquids for spent nuclear fuel reprocessing. In proceedings of the 12th International Conference on Microreaction Technology, 20–22 February, Lyon, France

Tsaoulidis D., Dore V., Plechkova N., Seddon K.R., Angeli P., 2012. Uranium extractions in small channels using ionic liquids. In proceedings of the Nuclear Fuel Cycle Conference, 23–25 April, Manchester, UK

Dore V., Tsaoulidis D., Angeli P., 2012. μ-PIV investigation of water/ionic liquid plug flow dynamics in meandering microchannels. In proceedings of 16th International Symposium on Applications of Laser Techniques to Fluid Mechanics, 09–12 July, Lisbon, Portugal

Tsaoulidis D., Dore V., Angeli, P., 2012. Extraction of U(VI) in microfluidic channels using ionic liquids. In proceedings of 3rd European Conference on Microfluidics, 03–05 December, Heidelberg, Germany

Tsaoulidis D., Li Q., Angeli, P., 2013. Hydrodynamics and mixing characteristics in small channels using ionic liquids for spent nuclear fuel reprocessing applications. In proceedings of the 8th International Conference on Multiphase Flow, Jeju, Korea, May 26–31

Tsaoulidis D., Li Q., Angeli, P., 2013. Flow characteristics of ionic liquid-aqueous two-phase flows in small channels. In proceeding of the 10th International Symposium on Particle Image Velocimetry, Delft, The Netherlands, July 1–3

Tsaoulidis D. & Angeli P., 2014. Spent nuclear reprocessing: Intensified extraction of $\{UO_2\}^{2+}$ in small channels using ionic liquids. Sustainable Nuclear Energy Conference 2014, Manchester, UK, April 9–11

Tsaoulidis D., Plechkova N., Seddon K. R., & Angeli P., 2014. $\{UO_2\}^{2+}$ extraction using ionic liquids in intensified extractors. Proceedings of the 22nd Interantional Conference on Nuclear Engineering 2014, Prague, Czech Republic, July 7–11

D.A. Tsaoulidis, *Studies of Intensified Small-scale Processes for Liquid–Liquid Separations in Spent Nuclear Fuel Reprocessing*,
Springer Theses, DOI 10.1007/978-3-319-22587-6

Tsaoulidis D., Li Q., Chinaud M., & Angeli P., 2014. Two-phase aqueous-ionic liquid flows in small channels of different diameter. 4th Micro and Nano Flows Conference, London, UK, September 7–10

Li Q., Tsaoulidis D., Angeli, P., 2014. Experimental and numerical investigations of ionic liquid-aqueous flows in small channels for europium recovery. In proceedings of 4rd European Conference on Microfluidics, 10–12 December, Limerick

Symposia

IChemE Fluid Separations Special Interest Group (FSSIG) annual research event "What's New in Fluid Separations?" at London Southbank University, London, UK, 8 June 2011. Dore V., Tsaoulidis D., Angeli P., 2011. "Two-phase liquid flows in microchannels for extraction applications"

IChemE Fluid Separations Special Interest Group (FSSIG) annual research event "What's New in Fluid Separations?" at Air Products Plc., European Technology Group, Basingstoke, Reading, UK, 16 May 2012. Tsaoulidis D., Dore V., Plechkova N., Seddon K.R., Angeli P., 2012 "Uranium extractions in small channels using ionic liquids." (Prize winner)

The Royal Academy of Engineering, Event: Next Generation Nuclear Energy- The UK's Role. 5 June 2013

Competitions

SET for BRITAIN March 17th 2014. "Green Solvents" for Intensified Spent Nuclear Fuel Reprocessing